Damping of 3D-printed polymer microbeam resonators

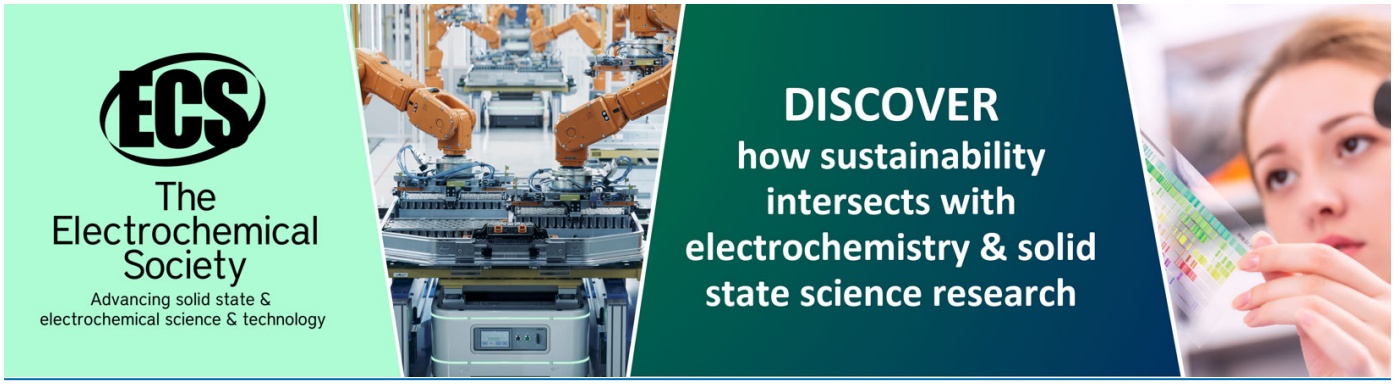

OPEN ACCESS
IOP Publishing
Journal of Micromechanics and Microengineering
J. Micromech. Microeng. **34** (2024) 015004 (9pp)
https://doi.org/10.1088/1361-6439/ad08ef

Damping of 3D-printed polymer microbeam resonators

Jikke de Winter[1], Tomás Manzaneque[2] and Murali Krishna Ghatkesar[1,*]

[1] Department of Precision and Microsystems Engineering, Delft University of Technology, Mekelweg 2, 2628 CD Delft, The Netherlands
[2] Department of Microelectronics, Delft University of Technology, Mekelweg 4, 2628 CD Delft, The Netherlands

E-mail: m.k.ghatkesar@tudelft.nl

Received 10 August 2023, revised 15 October 2023
Accepted for publication 2 November 2023
Published 28 November 2023

Abstract

The emerging high-resolution 3D printing technique called two-photon polymerization (2PP) enables to print devices bottom-up rapidly, contrary to the top–down lithography-based fabrication methods. In this work, various polymer microbeams are 3D printed and their resonant characteristics are analyzed to understand the origin of damping. The 2PP printed polymer resonators have shown less damping than other polymer devices reported earlier, with tensile-stressed clamped–clamped beams reaching a record quality factor of 1819. The resonant energy loss was dominant by bulk friction damping. These results pave the path towards using 3D printed microresonators as mass sensors with improved design and fabrication flexibility.

Supplementary material for this article is available online

Keywords: 3D printing, microresonator, additive manufacturing, damping, quality factor, polymer microbeam, 2PP printing

1. Introduction

Studying the physical characteristics of individual cells and sub-cellular components opens up new possibilities for advancements in biology and medicine. Research has demonstrated that properties like the mass and stiffness of cells are closely tied to various diseases [1–5]. For instance, blood cells and circulating tumor cells can be differentiated by assessing their deformability and mass [6]. Precise measurement of the mass of cells and subcellular components is possible by using micro- and nanomechanical resonant beams. These resonant beam sensors also find applications in various fields, including chemical sensing, biomolecular recognition, and humidity sensing [7–13].

Typically, microbeam resonators are fabricated out of silicon-based materials using photolithography technique. The technique is limited to producing 2D devices and very expensive to prototype devices in the design phase. Higher quality factor of resonance is a key factor in achieving a better mass resolution [14]. Polymers have distinct mechanical properties compared to silicon-based materials, with reduced device mass but also increased intrinsic damping. SU-8 polymer resonators were fabricated by lithography technique and high quality factors were achieved by inducing tensile stress in the beam [12]. Some groups have 3D printed microbeam resonators using two-photon polymerization (2PP) [10, 15]. This lithography-free technique enables rapid prototyping with a 3D design freedom, fabrication outside of an expensive cleanroom facility and ready to use devices without any further preparation steps after fabrication [10]. The damping behavior of 2PP printed microbeam resonators is not investigated so far.

* Author to whom any correspondence should be addressed.

In this work, we have 3D printed cantilevers and double-clamped beams with various dimensions, measured their resonant frequencies, identified major damping sources and compared them with existing theories. This systematic way of exploring damping is a novel approach to 3D printed microresonators and can serve as a step towards a wide range of applications. The current literature elaborately describes the damping of microresonators fabricated with lithography-based techniques or describes a single 3D printed microresonator without relating to damping theory or sweeping parameters. Furthermore, damping has been studied for polymer materials [16] but not specifically for 2PP fabricated materials. In addition to the systematic characterization of devices, our work demonstrates the reduction of damping by inducing tensile stress on a 3D printed double-clamped beam. This technique, previously used in non-polymeric devices, has been applied here to challenge the state-of-the-art of polymer microbeam resonators with low damping.

2. Methods and materials

2.1. Resonant beam fabrication

Solid resonators shaped like cantilevers and bridges were fabricated using 2PP 3D printing with the Professional GT (Nanoscribe GmbH & Co. KG, Germany). The structures were printed in Dip-in Laser Lithography configuration using 25× NA 0.8 lens (Carl Zeiss AG, Germany) in galvo mode at 100% (50 mW) laser power and 100 mm s^{-1} scanspeed using IP-S resin (Nanoscribe GmbH & Co. KG, Germany). IP-S was selected for its superior Young's modulus and other mechanical properties with respect to other IP materials. The structures were 3D printed on top of diced silicon wafer substrates with {100} orientation and the following dimensions: 25 mm long, 25 mm wide and 0.700 mm thick.

Two different types of microbeams were fabricated: thick beams with a thickness of 14 μm and thin beams with a thickness of 5 μm. Thick cantilevers and bridges are shown in figures 1(a) and (b). Thin type beam resonators are displayed in figures 1(c) and (d). Special thin type bridges were fabricated with a tapered width in the center to locally reduce the cross-sectional area. One of these devices is shown in figure 1(e). For this type of device, the width was narrowed down from 17.5 μm at the supports to 6 μm in the middle section. Table 1 displays the dimensions of the different structure types used for the measurements. Beam lengths were varied with steps of 50 μm. The beams were suspended from the substrate by rectangular pillars of the same material as the beams. Cantilevers and bridges were printed on the same substrate, with varying beam lengths (with steps of 50 μm). Two types of beams were printed with different printing methods. Thick beams were printed using block splitting in the longitudinal direction with square blocks of 4 μm × 4 μm with a 2 μm overlap. Thin beams were printed without block splitting.

The following development procedure was used for the printed structures: 25 min of submersion in ⩾99.5% Propylene glycol monomethyl ether acetate (MilliporeSigma, United States) followed by 30 s of submersion in Methoxy-nonafluorobutane known as Novec 7100 engineering fluid (MilliporeSigma, United States). Post-development thermal treatment of devices was performed at 200 °C for 15 min using the UN30 oven (Memmert GmbH + Co. KG, Germany), within the same day of characterization.

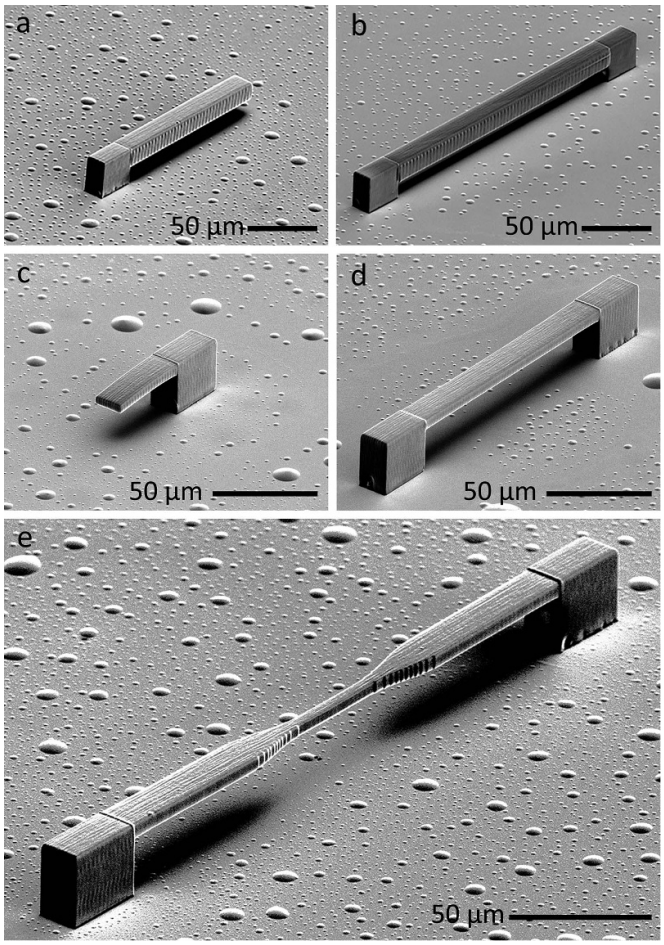

Figure 1. Scanning electron microscope pictures of fabricated IP-S microbeams with different geometries on a silicon substrate. (a) and (b) Thick type microbeams. (a) Cantilever 150 μm long, 17.5 μm wide and 14 μm thick. (b) Bridge 250 μm long, 17.5 μm wide and 14 μm thick. (c)–(e) Thin type microbeams. (c) Cantilever 50 μm long, 17.5 μm wide and 5 μm thick. (d) Bridge 150 μm long, 17.5 μm wide and 5 μm thick. (e) Narrowed bridge 250 μm long, 17.5 μm wide at the base, 6 wide μm at its center and 5 μm thick.

2.2. Resonator characterization

The resonant frequencies and corresponding quality factors of the solid beams were determined by laser Doppler vibrometry (MSA-400-PM2-D, Polytec GmbH, Germany). The samples were sputter-coated (JFC-1300) with approximately 72 nm of gold prior to the measurements, to increase the reflectivity of the devices surface. The samples were mounted on top of a piezoelectric actuator with a fundamental resonance frequency of approximately 4 MHz made of PIC255 (PI Ceramic GmbH, Germany) using double-sided carbon tape inside a homemade

Table 1. Design parameters of 3D structures that were printed.

Structure type	Length (μm)	Width (μm)	Thickness (μm)
Thick cantilever (figure 1(a))	50–300	17.5	14
Thick bridge (figure 1(b))	150–300	17.5	14
Thin cantilever (figure 1(c))	50–100	17.5	5
Thin bridge (figure 1(d))	100–300	17.5	5
Thin narrowed bridge (figure 1(e))	100–300	17.5 (base) 6 (center)	5
Pillar supporting beams (figures 1(a)–(e))	35	17.5	25

vacuum chamber. Single-point and multi-point measurements in frequency domain were performed and used to find the displacement peaks defining the resonant frequencies, and their corresponding modal shapes. A pseudo-random signal with white spectrum from 1 Hz to 2 MHz was used for driving the piezoelectric actuator, with a time-domain amplitude of 10 V. Measurements were performed at room temperature (20 °C) and high vacuum pressure ($\leqslant 5 * 10^{-5}$ mbar).

3. Results

3.1. Frequency spectra of 3D printed devices

The resonant frequency spectra of the fabricated devices was measured and their corresponding modal shapes were identified. Figure 2 shows the recorded resonant frequency spectrum of a bridge with a narrowed middle section. The different peaks are labeled with numbers. The peak with the highest magnitude (number 2) is considered as the fundamental resonant mode of the device. The remaining peaks, while having a qualitatively similar modal shape, present a considerable velocity (displacement) magnitude at the anchor points. Peak 1 with a lower resonant frequency has anchor points moving in phase with the center of the beam. Peaks 3 and 4 with a higher resonant frequencies have anchor points moving antiphase with the center, as pointed out with the black arrows. This behavior, exemplified by the device has been observed across all fabricated devices with less distinction. The origin of this phenomenon is discussed in section 4.1. The resonant peaks with a mode shape containing minimum displacement at the anchor points were considered as the fundamental resonant frequency for further analysis.

3.2. Quality factor of varying device dimensions and the effect of thermal treatment

The bulk friction damping has been shown to be the dominant damping phenomenon limiting the quality factors of most polymer microbeam resonators [12, 17], except for string-like microresonators. This material intrinsic damping is not only dependent on temperature and frequency, but also on the molecular structure of the polymer through the loss factor η. A preliminary experiment, described in the supplementary material, showed that post-development thermal and UV-exposure treatments in IP-S pillars leads to an increased Young's modulus. Therefore to improve the quality factor, microbeams were characterized after thermal treatment at

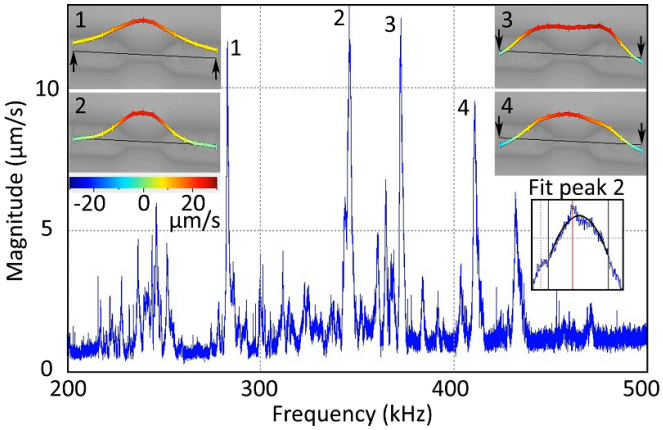

Figure 2. Frequency spectrum of a thin type narrowed bridge 200 μm long consisting of IP-S on a silicon substrate. Peaks are numbered and the associated modal shapes are displayed in the insets. Additionally, the fit of the resonance peak is displayed in inset 'fit peak 2'.

200 °C for 15 min. Thick and thin type cantilevers and bridges of varying lengths were characterized at high vacuum pressure ($\leqslant 5 \times 10^{-5}$ mbar).

The quality factors measured for thermally untreated and treated devices are plotted in figure 3. Each data point is obtained from an average of 5 devices that were measured. The error bar represents a standard deviation. In general, all devices showed an upwards trend in the quality factor with the resonant frequency, plateauing from around 200 kHz. The plots show that untreated cantilevers and bridges of both types have similar quality factor values at matching resonant frequencies. All thermally treated devices showed an increase in resonant frequency compared to untreated devices, this can be attributed to the increased Young's modulus (see supplementary materials). A small increase of the quality factor in general has been observed for thermally treated devices in comparison to untreated devices, except for the thick type cantilevers with 200 μm and 250 μm length. Those two thermally treated devices with a resonant frequency of around 100 kHz show a significantly lower quality factor compared to the untreated ones with the same length. The largest increase in quality factor is for the thin 200 μm bridge with 136 at 135 kHz without thermal treatment, to a quality factor of 506 at 181 kHz after thermal treatment. The highest quality factor in these experiments was for the thermally treated 100 μm long thick cantilever with 993 at 473 kHz.

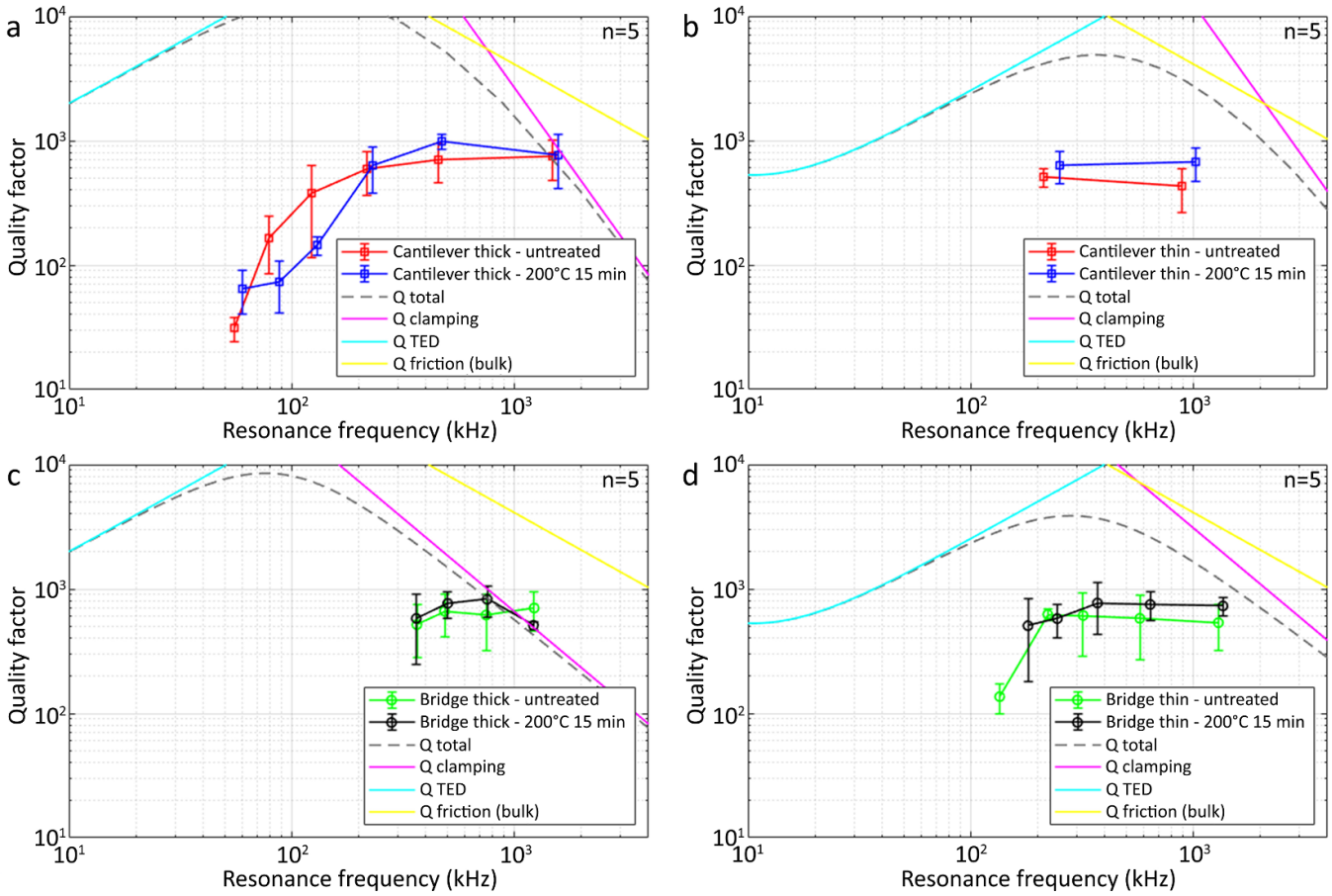

Figure 3. The quality factors of (a) thick cantilevers, (b) thin cantilevers, (c) thick bridges and (d) thin bridges, with and without thermal treatment. The solid lines with different colors represent theoretically calculated quality factors using equations given in Schmid *et al* [18] due to various damping sources. See also supplementary material for equations. The dashed line represents the total effective quality factor.

3.3. Modeling damping sources

Theoretical models for different damping phenomena are plotted together with the experimental data in figure 3. The applied models and their corresponding equations can be found in the supplementary material. The theoretical total damping is denoted by the dashed line, which can be calculated with equation (S.5) from the supplementary material. Theoretical values of Q_{medium} were in the order of 10^6, so they are out of range of the figure. The theoretical models of Q_{TED} and Q_{friction} are highly dependent on the material properties of IP-S, which can vary strongly with different fabrication parameters [19, 20]. The material properties used for modeling are shown in table 2. There is limited data available on the thermal and mechanical properties of IP-S, so the following assumptions and estimations were made in order to be able to plot models for thermoelastic damping and friction damping: unavailable data for IP-S was replaced by data of IP-DIP (indicated by * in the table 2) and the loss coefficient was conservatively estimated to be 0.1 from the literature [21].

Table 2. Material properties of IP-S used for theoretical models and calculations.

Material property	Value	Source
Young's modulus	2.3 GPa	Supplementary material
Relaxed Young's modulus*	2.6 GPa	[22]
Unrelaxed Young's modulus*	3.2 GPa	[22]
Loss coefficient	0.1	[21]
Mass density*	1189 kg m^{-3}	[19]
Thermal conductivity	0.3 W mK^{-1}	[23]
Coefficient of expansion	100×10^{-6} K^{-1}	[20, 23]
Heat capacity	1500 J kgK^{-1}	[23]

3.4. Thermal treatment of narrowed bridges

String-like polymer microbeam resonators have been reported to achieve the highest quality factors [12], especially when tensile stress was present in the longitudinal direction of the beam. The tensile stress in strings led to an increased quality factor [24] because this adds stored energy to the system, enhancing its proportion with respect to energy losses [16]. Following this idea, a narrowed middle section on a double-clamped resonator was used to locally increase stress by reducing the cross-sectional area, with the goal of enhancing the quality factor [25, 26]. Bridges were 3D printed with a narrowed middle section and thermally treated, in an attempt to create tensile stress by thermally inducing shrinkage, as

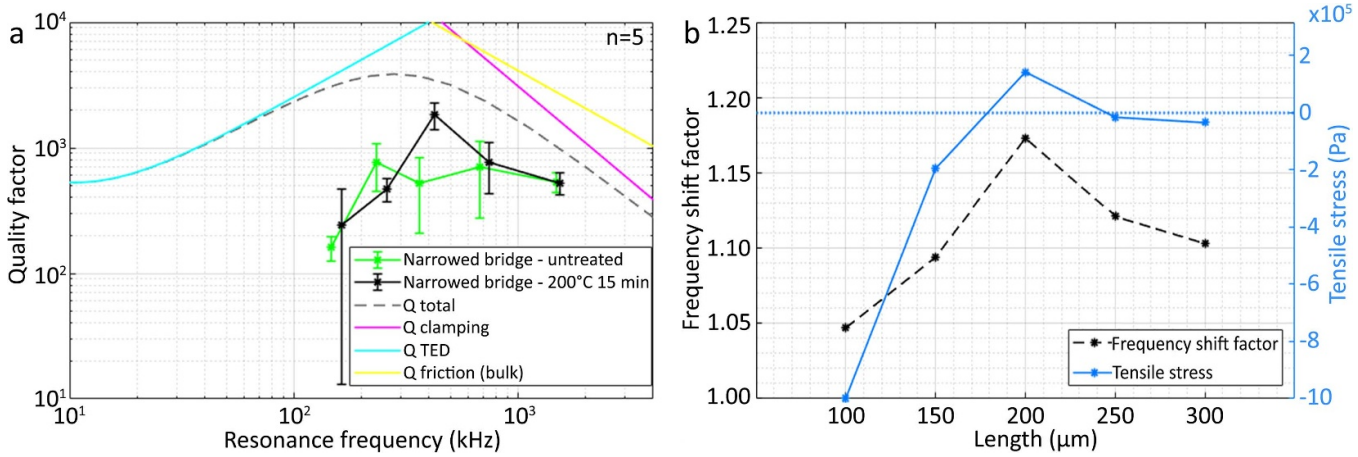

Figure 4. (a) Quality factor of thin type narrowed bridges with and without thermal treatment. The lines represent quality factor values obtained from theoretical models of different damping sources. (b) The dashed black line indicates the experimentally determined frequency shift factor F of thin type narrowed bridges of different beam lengths. The blue line indicates the tensile stress calculated with the analytical model based on the experimental determined F values.

observed in the preliminary experiment with pillars found in the supplementary material.

Results of this narrowed bridge experiment are plotted in figure 4(a), with further details found in the supplementary material. It can be seen that narrowed bridges with and without thermal post-development treatment (200 °C for 15 min) have similar quality factor values with one pronounced exception: the narrowed bridges with a length of 200 μm showed a significant increase in average quality factor, from 522 at 361 kHz for untreated beam to 1819 at 424 kHz after the thermal treatment. This value surpasses the highest quality factor reported for polymer microbeam resonators to the best of the authors' knowledge, 790 at 200 kHz for a stressed double-clamped beam [12]. An increase in resonance frequency was observed due to the treatment for narrowed bridges as shown in figure 4(a). The largest relative frequency increase was for the 200 μm long devices, which also showed a significant increase in quality factor. This could be an indication of significant tensile stress in this particular device. See section 4.3 for an explanation about why the length of 200 μm only showed a significant increase of the averaged quality factor.

An attempt to calculate the tensile stress in the narrowed bridges was performed, based on the experimentally observed shift in resonance frequency between untreated and treated devices using the methodology and assumptions described below. The following assumptions were made for the calculation of tensile stress: Conservation of device mass during thermal treatment, the internal stress of untreated beams is negligible, cross-section did not vary as a result of treatment, and beam length did not change by the treatment. The beam length is assumed constant because the beam anchor point's position is fixed to the surface of the substrate. The resonance frequency shift factor as a result of the thermal treatment will be denoted with F:

$$F = \frac{f_{R,\text{treated}}}{f_{R,\text{untreated}}}. \tag{1}$$

The resonant frequency of a double-clamped beam with tensile stress σ can be calculated using [27]

$$f_{R,n} = \frac{n^2\pi}{2l^2}\sqrt{\frac{YI}{\rho A}}\sqrt{1+\frac{\sigma A l^2}{YIn^2\pi^2}}. \tag{2}$$

Substituting $A = bh$ and $I = \frac{1}{12}bh^3$ ([28]) leads to:

$$f_{R,n} = \frac{n^2\pi}{2l^2}\sqrt{\frac{Yh^2}{12\rho}}\sqrt{1+\frac{12\sigma l^2}{Yh^2n^2\pi^2}}. \tag{3}$$

It should be noted that, besides the introduced stress, the Young's modulus, mass density and height are susceptible to being modified by the thermal treatment. The effect of these variables on the resonant frequency were accounted for using correction factor C_F, which can be calculated using equation (4). C_F was derived by substitution of equation (3) in equation (1), setting the stress to zero and using the Young's modulus, mass density and height as treatment variables

$$C_F = \frac{f_{R,n,\text{treated}}}{f_{R,n,\text{untreated}}} = \frac{\frac{n^2\pi}{2l^2}\sqrt{\frac{Y_{\text{treated}}h^2_{\text{treated}}}{12\rho_{\text{treated}}}}}{\frac{n^2\pi}{2l^2}\sqrt{\frac{Y_{\text{untreated}}h^2_{\text{untreated}}}{12\rho_{\text{untreated}}}}} = \frac{\sqrt{\frac{Y_{\text{treated}}h^2_{\text{treated}}}{\rho_{\text{treated}}}}}{\sqrt{\frac{Y_{\text{untreated}}h^2_{\text{untreated}}}{\rho_{\text{untreated}}}}}. \tag{4}$$

The values needed to evaluate equation (4) where obtained from the experiments with polymer pillars, as described in the supplementary material. Substituting equation (3) in equation (1) and correcting F through dividing it by the correction factor yields equation (5) for the tensile stress

$$\sigma_{n,\text{treated}} = \left(\left(\frac{F}{C_F}\right)^2 - 1\right) * \left(\frac{Y_{\text{treated}}h^2_{\text{treated}}n^2\pi^2}{12l^2}\right). \tag{5}$$

The local tensile stress in the narrowed part of the bridge was calculated with equation (6) [28].

$$\sigma_{\text{narrowed}} = \sigma_{n,\text{treated}} \frac{A}{A_{\text{narrowed}}}. \quad (6)$$

The frequency shift factor and the estimated tensile stress in thermally treated narrowed bridges are plotted in figure 4(b). According to the estimation, the 200 μm long devices, that showed a distinct quality factor increase, were the only ones with positive tensile stress induced by the thermal treatment (1.4×10^5 Pa).

4. Discussion

4.1. Origins of multiple resonance peaks

Fundamental resonant frequencies of the beams were identified by magnitude peaks and their matching mode shape. Multiple peaks with similar mode shapes were observed across all experiments, but only the peak with a mode shape containing minimum displacement at the anchor point(s) was selected to be the fundamental resonant frequency. Multiple resonant peaks with similar modal shapes is also known as 'forest of peaks' and has been reported before by others [29]. Coupling of the resonators with each other through the substrate could be argued to cause multiple peaks. Although the resonators fabricated on a single substrate had different fundamental resonant frequencies, different modes could still be coupled with the fundamental mode of another resonator fabricated on the same substrate. This cause was ruled out because the devices with the lowest fundamental resonant frequencies still had multiple peaks and fabricating a single beam per substrate did not solve the issue. 'Additional' resonant peaks with similar mode shapes but moving anchor points suggest a mechanical coupling between the beam and other resonating parts such as the piezoelectric transducer assembly, substrate or the anchor itself. Energy transfer through this coupling intensifies when the frequencies of substrate and resonator modes are closer together [30, 31]. This suggests that those 'additional' peaks are coupled substrate modes or anchor modes, which should not be fitted for characterization. Literature suggests that the resonances of the piezoelectric transducer (assembly) could also be the cause of the 'forest of peaks' phenomenon [32, 33]. Both causes agreed with the following unsuccessful attempts performed to solve this problem: Varying the excitation voltage, performing single point measurement, changing anchor geometry, varying distance from beam to the substrate, eliminating block splitting of beams or fabricating a single beam per substrate.

4.2. Discrepancy between damping models and experimental results

The theoretical damping models shown in figure 3 did not fit the experimental data across all devices. The models of thermoelastic damping and friction damping are highly dependent on material properties, which were partly undetermined and can vary strongly with fabrication parameters [19, 20]. The high uncertainty of the values of material properties used in these models explains the mismatch between theory and experiments. In an attempt to reconcile this problem, unavailable data for IP-S was replaced by data of IP-DIP for the following material properties: relaxed Young's modulus, unrelaxed Young's modulus and mass density. In order to improve the accuracy of the models, the following material properties would be necessary: relaxed Young's modulus, unrelaxed Young's modulus, mass density, loss coefficient, thermal conductivity, coefficient of expansion and heat capacity. Another approach to improve the accuracy of the models is to tune the material properties to make the models fit the experimental data. Unfortunately, fitting the models to experimental data was not possible without significant corrections on the values of material properties. This makes it a trivial exercise also considering the higher number of variables. Finally, the bulk friction damping model was based on a single relaxation time in contrast to the case of a real polymer, which has multiple relaxation times [34]. These were enough reasons not to take the quality factor values of the theoretical models into account during the determination of the dominant damping phenomenon, but only their theoretical dependencies.

4.3. Dominant damping source

The fundamental question of finding the dominant damping source(s) of our polymer microbeam resonators was answered by eliminating damping sources one by one (see equation (S.5) in the supplementary material). Experimental results and theoretical models are compared in order to eliminate possible dominant damping sources based on their theoretical dependencies. In order to be able to single out damping sources, the following variations were introduced in the devices fabricated: beam length (resonant frequency), beam thickness and clamping type.

The quality factor values of thermoelastic damping are dependent on beam thickness, which is also displayed by the model used in figure 3. The experimental results show that changing the thickness of beams does not affect the quality factor values at matching resonant frequencies. This suggests that thermoelastic damping can be eliminated as dominant damping source in our devices. The modeled quality factor for clamping loss of beams are significantly different for cantilevers and bridges, and a strong dependence with beam thickness is expected (see equations (S.8) and (S.9) in the supplementary material). In our experiments, cantilevers and bridges showed similar quality factors at matching resonant frequencies for both thick and thin devices, suggesting that clamping damping can also be eliminated as dominant damping source. Estimations for medium interaction damping at the pressure set in our experiments indicate quality factors being three orders of magnitude higher than the quality factors measured. Schmid [27] showed experimentally that the influence of air damping vanishes for devices of comparable dimensions with pressures below (10^{-1} mbar). After eliminating damping sources based on their theoretical dependencies and the experimental results, bulk friction damping is left as the dominant damping source for our devices.

4.4. Effects of thermal treatment on quality factor

Quality factors of cantilevers and bridges with constant cross section, dominated by friction damping, did not change significantly by post-development thermal treatment at 200 °C for 15 min, even though Young's modulus changed by a factor of 1.5. This suggests that the friction damping has not changed significantly by the expected increase in cross-links between polymer chains.

High frequency shift and quality factor increase were observed for the 200 μm long narrowed bridges. This not only indicated that tensile stress was present in devices with these dimensions ($n = 5$), but that locally increasing this stress by reducing the cross-sectional area led to enhanced stored energy with respect to the damping, therefore significantly increasing the quality factor [16, 24]. This demonstrated a successful case of strain engineering because only a small increase in quality factor was observed for the thin type bridges (without narrowing) of 200 μm length with the same thermal treatment. Although simulations verified that a frequency shift factor above 1.13 is caused by positive tensile stress in the beam, it did not give an explanation to why only 200 μm long devices showed it. It is suspected that plastic deformation entailing negative tensile stress was induced in the beams during development and prior to the thermal treatment. This is supported by the observation that narrowed bridges were slightly bent down towards the surface of the substrate after fabrication, see the supplementary material, supposedly caused by capillary forces exerted by the evaporating development liquid [35]. This plastic deformation is more pronounced for longer beams due to their lower stiffness and larger area of interaction with the liquid meniscus during drying. The bending of the device has a competing effect with the length dependency of induced (positive) tensile stress by volumetric shrinkage. Increasing tensile stress should be induced for longer beams, assuming uniform shrinkage, fixed anchor points and constant cross-sectional area for different beam lengths.

The combination of the two competing effects might leave long beams too deformed to shrink enough to induce positive tensile stress and short beams with not enough longitudinal shrinkage to induce positive tensile stress. This can explain the local maximum in the frequency shift factor as a function of the beam length, with the consequent maximum in the estimated stress. Such remnants of the fabrication processes are something to consider when using them but do not provide a broader understanding for polymer microbeam resonators.

4.5. Comparison with state of the art

The quality factors of the devices in this work have exceeded the state of the art of polymer microbeam resonators. Figure 5 provides a comparison between the previously reported quality factor values with the values demonstrated in this work, as a function of the resonance frequency. he figure shows that the 3D printed devices in this work approach quality factors of 1000, generally outperforming previously reported polymer microbeam resonators in a resonance frequency range from 60 kHz to 1500 kHz. There is a single exception reported by Schmid *et al*, the stressed bridge with a quality factor of 790 at 200 kHz [16]. Outperforming previously reported polymer microbeam resonators can be attributed to the reduction of medium interaction damping by characterizing at high vacuum pressure ($\leqslant 5 * 10^{-5}$ mbar) and achieving reduced friction damping. The reduced friction damping could be caused by a smaller loss coefficient η of the material, or by the resonance frequencies being far away from the inverse of the material relaxation rate $\bar{\tau}$ (see equation (S.12)). The tensile-stressed narrow bridges achieved a quality factor of 1819, providing a significant improvement by utilizing the induced tensile stress to add stored energy to the system, enhancing its proportion with respect to energy losses.

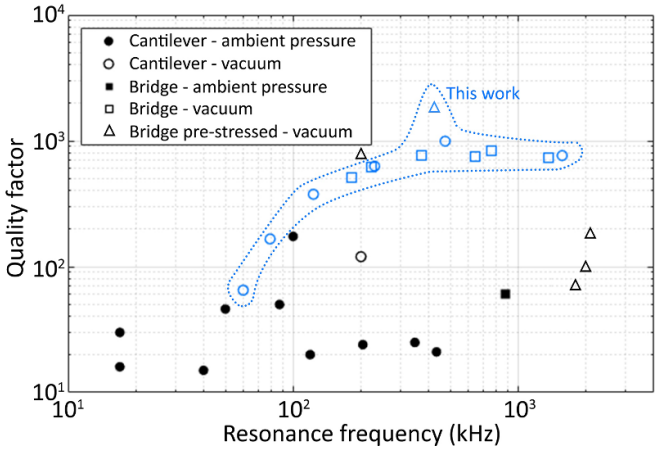

Figure 5. State of the art of the quality factor of polymer microbeam resonators, with devices from this work in blue [7–10, 15, 17, 27, 36–41].

5. Conclusion

The goal of this work was to understand the origin of damping in 3D printed polymer microbeam resonators and maximize their quality factor. The 3D printed devices from this work set a new quality factor standard among polymer microbeam resonators. Cantilevers and bridges characterized at high vacuum pressure ($\leqslant 5 * 10^{-5}$ mbar) approached quality factors of 1000. Additionally, a method for improving the quality factor of polymer beam resonators was investigated. Our results and analysis show that shrinkage by thermal post-development treatment can be utilized to create tensile stress and improve the quality factor. In our case, this technique has lead to a quality factor of 1819 in bridges with narrowed cross section. The relevant question of what is the dominant damping source in our 3D printed polymer beams was answered by discarding possible damping sources based on experimental results and their theoretical dependencies. The conclusion is that bulk friction damping is the dominant damping source for all devices. These results pave the path towards using 3D printed microresonators as mass sensors with additional design and fabrication flexibility.

Data availability statement

All data that support the findings of this study are included within the article (and any supplementary files). The data that supports the findings of this study are available from the corresponding author upon reasonable request.

Acknowledgments

The authors would like to thank Pieter van Altena and Ahmed Sharaf for the training and lab brainstorming sessions. They also like to thank the PME lab staff members Gideon Emmaneel and Patrick van Holst for their practical support. This work is part of the research project titled NFP4CryoEM with Project Number 13711, which is (partly) funded by the Netherlands Organisation for Scientific Research (NWO-STW). Tomás Manzaneque acknowledges funding from the European Union's Horizon 2020 research and innovation programme under the Marie SkłodowskaCurie Grant Agreement No. 707404. The opinions expressed in this document reflect only the authors' views. The European Commission is not responsible for any use that may be made of the information it contains.

ORCID iDs

Jikke de Winter https://orcid.org/0009-0003-1812-7720
Tomás Manzaneque https://orcid.org/0000-0002-1738-4261
Murali Krishna Ghatkesar https://orcid.org/0000-0001-8423-3159

References

[1] Cross S E, Jin Y-S, Rao J and Gimzewski J K 2007 Nanomechanical analysis of cells from cancer patients *Nat. Nanotechnol.* **2** 780–3
[2] Greber U F 2016 Virus and host mechanics support membrane penetration and cell entry *J. Virol.* **90** 3802–5
[3] Suresh S, Spatz J Mills J, Micoulet A, Dao M, Lim C, Beil M and Seufferlein T 2015 Reprint of: connections between single-cell biomechanics and human disease states: gastrointestinal cancer and malaria *Acta Biomater.* **23** S3–S15
[4] De Pastina A and Villanueva L G 2020 Suspended micro/nano channel resonators: a review *J. Micromech. Microeng.* **30** 043001
[5] Gil-Santos E, Ruz J J, Malvar O, Favero I, Lemaître A, Kosaka P M, García-López S, Calleja M and Tamayo J 2020 Optomechanical detection of vibration modes of a single bacterium *Nat. Nanotechnol.* **15** 1–6
[6] Byun S *et al* 2013 Characterizing deformability and surface friction of cancer cells *Proc. Natl Acad. Sci.* **110** 7580–5
[7] Calleja M, Nordström M, Álvarez M, Tamayo J, Lechuga L M and Boisen A 2005 Highly sensitive polymer-based cantilever-sensors for dna detection *Ultramicroscopy* **105** 215–22
[8] Genolet G, Brugger J, Despont M, Drechsler U, Vettiger P, De Rooij N and Anselmetti D 1999 Soft, entirely photoplastic probes for scanning force microscopy *Rev. Sci. Instrum.* **70** 2398–401
[9] Urwyler P, Schift H, Gobrecht J, Häfeli O, Altana M, Battiston F and Müller B 2011 Surface patterned polymer micro-cantilever arrays for sensing *Sens. Actuators* A **172** 2–8
[10] Kramer R C, Verlinden E J, Angeloni L, Van Den Heuvel A, Fratila-Apachitei L E, Van Der Maarel S M and Ghatkesar M K 2020 Multiscale 3d-printing of microfluidic afm cantilevers *Lab Chip* **20** 311–9
[11] van Altena P F J 2021 Multiscale 3D printed polymer probes for single cell experiments *Master's thesis* TU Delft, Delft
[12] Schmid S and Hierold C 2008 Damping mechanisms of single-clamped and prestressed double-clamped resonant polymer microbeams *J. Appl. Phys.* **104** 093516
[13] Schmid S, Wägli P and Hierold C 2008 All-polymer microstring resonant humidity sensor with enhanced sensitivity due to change of intrinsic stress *Proc. of the Eurosensors XXII conf.* (*Dresden, Germany*) pp 697–700
[14] Burg T P, Mirza A R, Milovic N, Tsau C H, Popescu G A, Foster J S and Manalis S R 2006 Vacuum-packaged suspended microchannel resonant mass sensor for biomolecular detection *J. Microelectromech. Syst.* **15** 1466–76
[15] Frehner L and Maillard D 2018 Optimization of channel design and fabrication for suspended microchannels resonators with a 3d nanoprinter *Technical Report* (Ecole Polytechnique Fédérale de Lausanne)
[16] Schmid S, Jensen K, Nielsen K and Boisen A 2011 Damping mechanisms in high-q micro and nanomechanical string resonators *Phys. Rev.* B **84** 165307
[17] Zhang G, Chu V and Conde J P 2007 Conductive blended polymer mems microresonators *J. Microelectromech. Syst.* **16** 329–35
[18] Schmid S, Villanueva L G and Roukes M L 2016 *Fundamentals of Nanomechanical Resonators* vol 49 (Springer)
[19] Lemma E D, Rizzi F, Dattoma T, Spagnolo B, Sileo L, Qualtieri A, De Vittorio M and Pisanello F 2016 Mechanical properties tunability of three-dimensional polymeric structures in two-photon lithography *IEEE Trans. Nanotechnol.* **16** 23–31
[20] Huang W and de Payrebrune K M 2019 Experimental investigation on the thermal length expansion of direct laser writing material *Proc. Appl. Math. Mech.* **19** e201900485
[21] Ashby M F 1989 Overview no. 80: On the engineering properties of materials *Acta Metall.* **37** 1273–93
[22] Rohbeck N, Ramachandramoorthy R, Casari D, Schürch P, Edwards T E, Schilinsky L, Philippe L, Schwiedrzik J and Michler J 2020 Effect of high strain rates and temperature on the micromechanical properties of 3D-printed polymer structures made by two-photon lithography *Mater. Design* **195** 108977
[23] Babaei M, Kim S, Velez C, Patel D K and Bergbreiter S 2020 Increasing the energy efficiency of NiTi unimorph actuators with a 3D-printed passive layer *J. Microelectromech. Syst.* **29** 797–803
[24] Verbridge S S, Parpia J M, Reichenbach R B, Bellan L M and Craighead H G 2006 High quality factor resonance at room temperature with nanostrings under high tensile stress *J. Appl. Phys.* **99** 124304
[25] Minamisawa R A, Süess M J, Spolenak R, Faist J, David C, Gobrecht J, Bourdelle K K and Sigg H 2012 Top-down fabricated silicon nanowires under tensile elastic strain up to 4.5% *Nat. Commun.* **3** 1–6
[26] Ghadimi A H, Fedorov S A, Engelsen N J, Bereyhi M J, Schilling R, Wilson D J and Kippenberg T J 2018 Elastic strain engineering for ultralow mechanical dissipation *Science* **360** 764–8

[27] Schmid S 2009 *Electrostatically Actuated All-Polymer Microbeam Resonators: Characterization and Application* vol 6 (ETH Zurich)
[28] Hibbeler R C 2005 *Mechanics of Materials* (Pearson Educación)
[29] Desbiolles B X, Furlan G, Schwartzberg A M, Ashby P D and Ziegler D 2018 Electrostatically actuated encased cantilevers *Beilstein J. Nanotechnol.* **9** 1381–9
[30] Zanette D H 2018 Energy exchange between coupled mechanical oscillators: linear regimes *J. Phys. Commun.* **2** 095015
[31] de Jong M H J, ten Wolde M A, Cupertino A, Gröblacher S, Steeneken P G and Norte R A 2022 Mechanical dissipation by substrate–mode coupling in sin resonators *Appl. Phys. Lett.* **121** 032201
[32] Carrasco C, Ares P De Pablo P and Gómez-Herrero J 2008 Cutting down the forest of peaks in acoustic dynamic atomic force microscopy in liquid *Rev. Sci. Instrum.* **79** 126106
[33] Kokavecz J and Mechler A 2007 Investigation of fluid cell resonances in intermittent contact mode atomic force microscopy *Appl. Phys. Lett.* **91** 023113
[34] Young R J and Lovell P A 2011 *Introduction to Polymers* (CRC Press)
[35] Legtenberg R, Tilmans H A, Elders J and Elwenspoek M 1994 Stiction of surface micromachined structures after rinsing and drying: model and investigation of adhesion mechanisms *Sens. Actuators* A **43** 230–8
[36] McFarland A W, Poggi M A, Bottomley L A and Colton J S 2004a Production and characterization of polymer microcantilevers *Rev. Sci. Instrum.* **75** 2756–8
[37] McFarland A W, Poggi M A, Bottomley L A and Colton J S 2004b Injection moulding of high aspect ratio micron-scale thickness polymeric microcantilevers *Nanotechnology* **15** 1628
[38] Xu T, Bachman M, Zeng F-G and Li G-P 2004 Polymeric micro-cantilever array for auditory front-end processing *Sens. Actuators* A **114** 176–82
[39] Mouaziz S, Boero G, Popovic R S and Brugger J 2006 Polymer-based cantilevers with integrated electrodes *J. Microelectromech. Syst.* **15** 890–5
[40] Accoto C, Qualtieri A, Pisanello F, Ricciardi C, Pirri C F, De Vittorio M and Rizzi F 2014 Two-photon polymerization lithography and laser doppler vibrometry of a su-8-based suspended microchannel resonator *J. Microelectromech. Syst.* **24** 1038–42
[41] Hosseini N, Neuenschwander M, Peric O, Andany S H, Adams J D and Fantner G E 2019 Integration of sharp silicon nitride tips into high-speed su8 cantilevers in a batch fabrication process *Beilstein J. Nanotechnol.* **10** 2357–63